Studying the strength and damageability of composite element in looped metal-composite joint under tensile loading

Irakly Kacharava, Tatiana Ryzhova, Vladimir Vermel, Alexander Shanygin, Danil Fomin, Yury Mirgorodsky, Nikolay Kovalyov
Central Aerohydrodynamic Institute named after Professor N.E. Zhukovsky, Russian Federation
irakliy.kacharava@tsagi.ru
tatiana.ryzhova@tsagi.ru, https://orcid.org/0000-0003-0242-0159
npk@tsagi.ru
alexander.shanygin@tsagi.ru, https://orcid.org/0000-0002-1389-7924
denver2613@yandex.ru, https://orcid.org/0000-0001-9931-4701
yuriy.mirgorodskiy@tsagi.ru, https://orcid.org/0000-0003-4449-6290
nikolay.kovalev@tsagi.ru

Yulia Petronyuk, Vadim Levin
Emanuel Institute of Biochemical Physics of the Russian Academy of Sciences, Russian Federation
jps7@mail.ru, https://orcid.org/0000-0002-9187-5288
levin1943@google.com

Sergey Lekomtsev
Institute of Continuous Media Mechanics of the Ural Branch of the Russian Academy of Sciences, Russian Federation
lekomtsev@icmm.ru, https://orcid.org/0000-0002-8331-2979

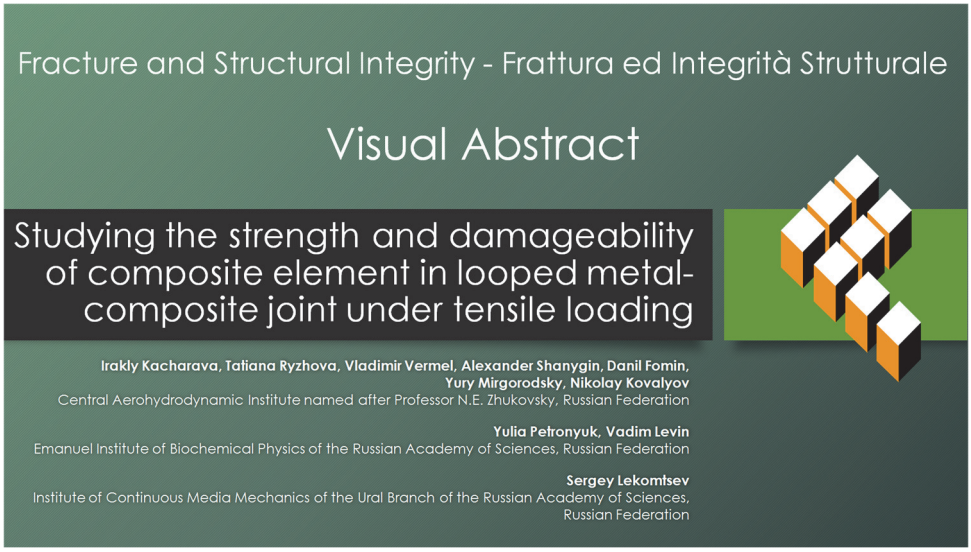

KEYWORDS. Aircraft structures, Polymer composite materials, Carbon fiber reinforced polymers, Metal-composite joint, Finite element method, Acoustic microscopy.

Citation: Kacharava, I., Ryzhova, T., Vermel, V., Shanygin, A., Fomin, D., Mirgorodsky, Yu., Kovalyov, N., Petronyuk, Yu., Levin, V., Lekomtsev, S., Studying the strength and damageability of composite element in looped metal-composite joint under tensile loading, Fracture and Structural Integrity, 74 (2025) 193-205.

Received: 14.07.2025
Accepted: 20.08.2025
Published: 28.08.2025
Issue: 10.2025

Copyright: © 2025 This is an open access article under the terms of the CC-BY 4.0, which permits unrestricted use, distribution, and reproduction in any medium, provided the original author and source are credited.

INTRODUCTION

In modern conditions, the use of polymer composite materials (PCMs) in aircraft structures is significantly expanded [1, 2]. This is due to the high specific strength of PCMs, which exceeds, in particular, that of aviation aluminum alloys by 4–5 times. However, despite their higher specific strength, it is not possible to achieve a corresponding reduction in structure mass. The main reason for this is the low deformation and strength properties of the polymer binder that forms a matrix into which threads or woven reinforcing filler materials made from glass or carbon fibers are placed. The high mechanical properties of PCMs are primarily provided in the directions determined by the orientation of the threads. In this regard, traditional design and technological solutions do not allow for the full realization of PCM's high mechanical properties.

One of the ways to overcome this problem is the development and application of so-called pro-composite structural design, which maximizes the advantages of PCM [3–8]. Effective structural designs are spatial isogrid structures formed by intersecting stiffeners based on a reinforcing filler with unidirectional loading, which coincides with the orientation of the filler threads. In the history of aviation, the Vickers Wellington aircraft is known for its extensive use of isogrid metallic construction in the wing and fuselage frame. Samples of isogrid frames made of composite material for the Boeing B-757 and B-767 long-range passenger aircraft were manufactured in the early 1980s. The first demonstrator of the composite isogrid fuselage structure focused on the USSR IL-114 regional passenger aircraft was manufactured in the late 1980s [4]. Despite of the first long range aircrafts with composite structures were made by using traditional semi-monocoque layouts, a lot of projects connected with perspective civil aircraft structures are aimed at development of isogrid structures.

The load-bearing elements of this design are located along the geodetic lines of the surface. For a fuselage similar to a cylinder in shape, they are formed by helical lines (spirals) and circles that form a mesh structure with joints at points where the stiffeners intersect. Mesh structures can withstand bending and torsional forces, as well as shear forces. A schematic view of the general design of the technological demonstrator for an isogrid structure is shown in Fig. 1. Bending moments are also perceived by longitudinal load-bearing elements of the structure – the fuselage beams. An isogrid design for PCM production differs from a traditional design in terms of higher strength, rigidity, and relatively lower weight [8–10]. Unification of individual structural components into airframe assemblies is performed using metal-composite detachable joints [9, 10].

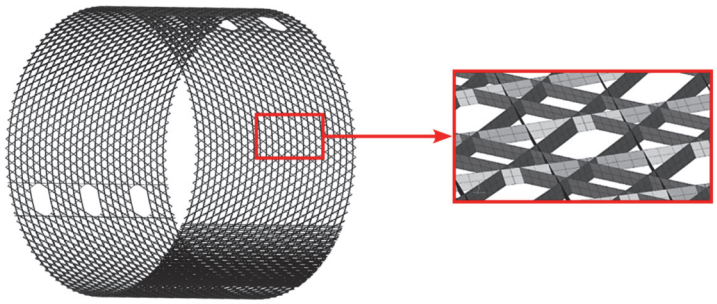

Figure 1: General view of the technological demonstrator of the composite fuselage part and a fragment of the isogrid structural design.

The article presents the results of a computational and experimental study aimed at evaluating the strength properties of a composite connecting element (loop) as part of a prototype metal composite joint, as well as the effect of load on the distribution of local stresses and structural damages. Similar studies have been conducted for bolted [11] and adhesive [12, 13] joints. It turned out to be difficult to find published works devoted to the study of metal-composite joint (MCJ) in the form of loops, but there are papers devoted to studying damage of mesh structures themselves [14]. Our publication allows to add to these by understanding the strength of a MCJ with a composite loop element. It contains both theoretical calculations, including those obtained using the finite element method, and experimental observations of the MCJ behavior under tensile loading. Examples and principles for using finite element method (FEM) to design and optimize composite mesh structures and MCJs can be found in [13, 15].

Taking into account the features of damage of reinforced polymers under external influences, which is the formation of multiple sources of damage at the micro-level, a study of the state of the composite part's structure of MCJ was conducted

before and after loading using non-destructive method of three-dimensional visualization. Generally, X-ray computed tomography and ultrasonic methods are successfully used for this purpose [16–23]. We applied acoustic microscopy (AM) to detect the development of microscopic damage from early stages of mechanical loading in our study.

DESIGN CALCULATION OF THE METAL-COMPOSITE JOINT PROTOTYPE

Possible options for connecting the components of the PCM structure in a meshed isogrid design are shown in Fig. 2. These include connecting the composite part of the structure to a composite, metal to a composite material, and a fragment of a metal-composite butt joint. The joints of the structural components use the same type of metal-composite joint shown in Fig. 2b. This is implemented in a prototype of a structurally similar sample. The design developed for the prototype which provides loading of a composite part in our experiment is similar to that used in the joints shown in Fig. 2. The detailed design of the metal-composite joint prototype is shown in Fig. 3.

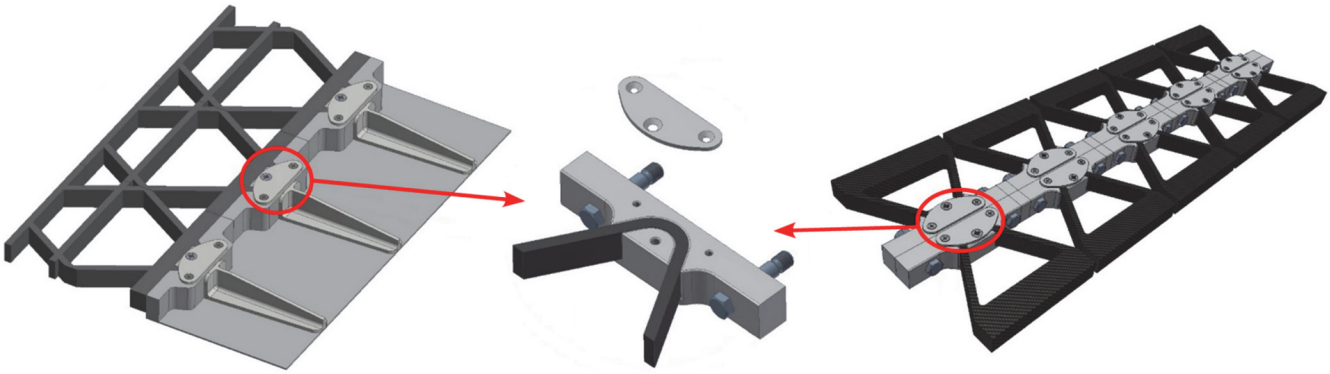

Figure 2: General view of the PCM structure components connection: a) the connection of the composite structure of the isogrid structural design; b) a fragment of the butt joint; c) the connection of the isogrid with the metal structure.

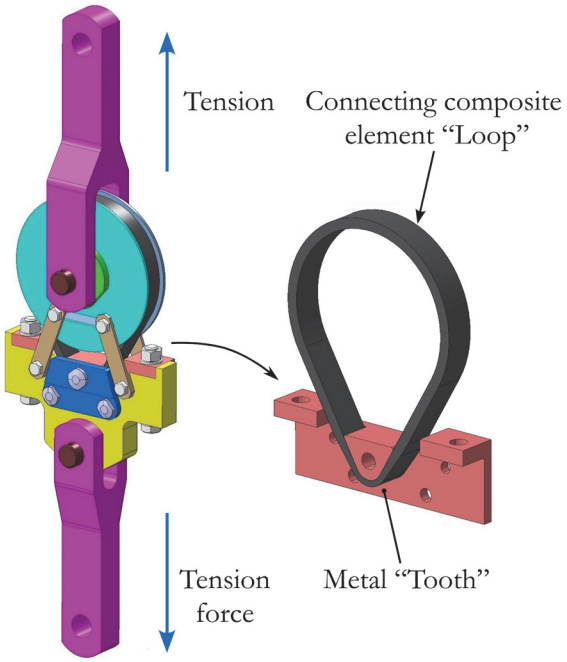

Figure 3: General view of a structurally similar sample assembly and a separated fragment of a metal-composite joint: connecting composite element – regular cross-section (Loop) and minimal cross-section (Tooth).

The main composite part in the prototype of a structurally similar sample of a metal-composite joint (Fig. 3) is made of unidirectional carbon fiber using tape winding technology − a detail in the form of a closed "loop". The general view of the connecting composite element of the MCJ and the properties of the composite material are shown in Tab. 1. The composite "loop" has a constant height of 30 mm and a variable thickness (6.55–10 mm). The reduction in the thickness of the "loop" was achieved by compressing the material during the manufacture of the sample to locally reduce the percentage of binder and increase the local strength of the composite element in the contact zone with the metal part of the MCJ.

Before manufacturing, the design calculations and subsequent modeling of the composite parts using the finite element method were carried out, including assessment of maximum destructive loads and the stress-strain state in the regular zone during stretching and crumpling of the composite material at the minimum cross-section of the loop. The physical and mechanical properties of IMS-65 E23 24K 830tex fibers used for calculations are given in Tab. 2.

Parameter	Value
Reinforcement	Carbon fibers IMS-65 Toho Tenax
Binder	Epoxy polymer ED-20
Reinforcing technology	Winding, fiber laying scheme [0°]
Volume content of fibers v_f	51.4%
Volume content of binder v_m	48.6%

Table 1: Material parameters of the MCJ composite elements in a regular section.

Parameter	Value
Number of microfibers in a thread	24000
Fiber density ρ, g/cm^3	1.78
Diameter of microfiber d, μm	5
Tensile strength of microfiber σ_{mf}, MPa	6000
Elastic modulus of microfiber E_{mf}, MPa	290000

Table 2: Physical and mechanical properties of the reinforcement.

The strength σ_f and elastic modulus E_f of the fiber (formed from 24000 microfibers) were obtained using the "Rule of Mixtures" [3]:

$$\sigma_f = \sigma_{mf} v_{mf} + \sigma_m v_m, \quad E_f = E_{mf} v_{mf} + E_m v_m, \tag{1}$$

where v_{mf} is the relative volume of microfibers, v_m is the relative volume of the binder matrix. The "Rule of Mixtures" based on the iso-strain assumption is a simplified but widely used approach for estimating the longitudinal stiffness and strength of unidirectional composites. It provides a reasonable first-order approximation, especially for high-modulus fiber composites with perfect bonding. Considering that the "Loop" is made of a unidirectional high-modulus composite, the application of the rule of mixture is justified.

Considering that the binder has an order of magnitude lower properties (tensile strength σ_m and elastic modulus E_m of binder matrix) than the fibers of the reinforcing filler, we will exclude it from consideration here and further. This simplification is used as a safety margin, and formula (1) will take the following form:

$$\sigma_f = \sigma_{mf} v_{mf}, \quad E_f = E_{mf} v_{mf}. \tag{2}$$

According to Fig. 4, the relative volume of microfibers v_{mf} can be estimated as the ratio of the circle area with a fiber diameter d to the area of an outlined square with side d:

$$v_{mf} = \left(\pi d^2/4\right)\Big/ d^2 = \pi/4. \tag{3}$$

In regular parts of the isogrid structure fiber volume ratio isn't higher than 40%. This restriction is caused by another restriction connected with maximum fiber volume ratio equals 70–80% in intersections of ribs. In this case, height and width of ribs in intersections could be the same as in regular parts of ribs. For this reason, the elementary cell scheme (shown in Fig.4) was chosen.

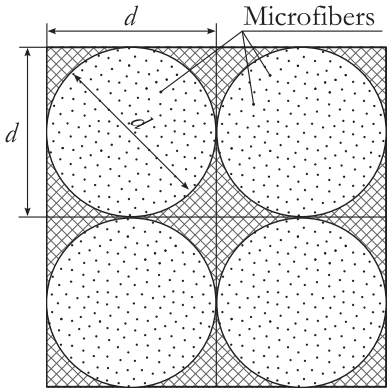

Figure 4: The scheme is an elementary cell of the minimum cross-section of the composite "loop", with compressed in the production process, packaging of reinforcing filaments. The same approach applies to the cross-section of a single reinforcing filament composed of microfibers.

Since the loop is made of unidirectional composite fibers, similarly, it is possible to estimate the relative volume of the reinforcing filler in the minimum section of the loop, consisting of carbon filaments pressed together into a compressed package during the molding of the composite (Fig. 4):

$$v_f = \left(\pi d^2/4\right)\Big/ d^2 = \pi/4. \tag{4}$$

Taking into account the insignificance of the influence of the binder in the fiber-to-fiber space, the tensile strength σ_{min} and stiffness modulus E_{min} of the "loop" in the minimum cross-section are estimated by the ratios similar to (2), taking into account equation (4):

$$\sigma_{min} = \sigma_f \pi/4, \quad E_{min} = E_f \pi/4. \tag{5}$$

The tensile strength σ_{reg} and stiffness modulus E_{reg} in a regular section of a carbon fiber "loop" in combination with an epoxy binder are estimated using a formula similar to (2), taking into account the volume composition of the fiber and binder shown in Tab. 1:

$$\sigma_{reg} = \sigma_{min} v_f, \quad E_{reg} = E_{min} v_f. \tag{6}$$

Parameter	Value, MPa	Formula
Tensile strength of a single filament σ_f	4712	(2)
Elastic modulus of a single filament E_f	227766	
Tensile strength in minimal section σ_{min}	3629	(5)
Elastic modulus in minimal section E_{min}	178887	
Tensile strength of a single filament σ_{reg}	1863	(6)
Elastic modulus of a single filament E_{reg}	91948	

Table 3: Physical and mechanical properties of the reinforcement.

Tab. 3 shows the calculation results. It can be seen that the tensile strength σ_{min} at the minimum section of "loop" is 3629 MPa, which is approximately twice that of the regular section's tensile strength 1863 MPa. Using the data in Tab. 3,

the maximum value of tensile load P_{max} (250 kN) was obtained for experimental verification of the strength of the MCJ prototype in the most loaded area with minimum cross-section, where composite contacts metal. This value was three times lower than the calculated one considering the minimum cross-sectional area of the sample of 200 mm².

The following geometric parameters of the composite elements were realized for metal-composite joint prototype sample:

- area of the regular cross-section S_{reg} = 300 mm² (10×30 mm);
- area of minimum cross-section S_{min} ≈ 197 mm² (6.4×30 mm);
- overall dimensions of the sample: 188×253 mm.

The geometric parameters of MCJ metal parts were also calculated. The designed sample, shown in Fig. 3, was manufactured and prepared for strength tensile testing.

TENSILE TESTING OF A METAL-COMPOSITE JOINT SAMPLE

The purpose of testing the metal-composite joint sample was to study the effect of tensile load on the damage of the composite connecting element in the form of a "loop". Tensile loads were applied as shown in Fig. 3. Ten load cells were installed on the composite tape (Fig. 5). Special attention was paid to the minimum cross-sectional area of the loop. When the MCJ specimen was loaded, the contact area between the composite "loop" and the metal "tooth" experienced different mechanical effects: unidirectional carbon fibers stretched in the regular area and compressed in contact with the metal. Loading of the MCJ samples was carried out on an LT TM-1000 testing machine with rate 1 kN/s.

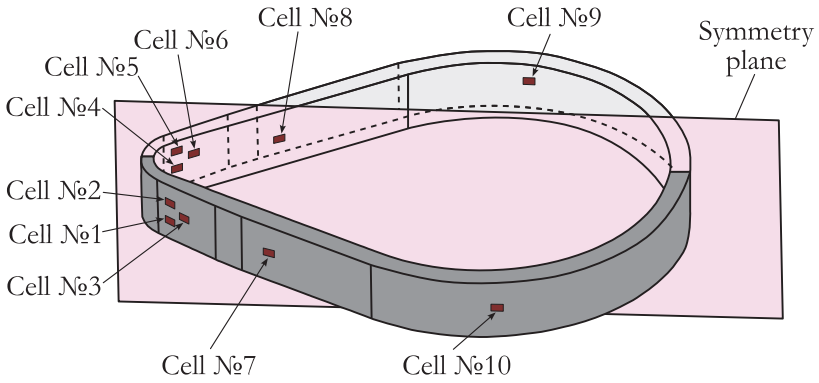

Figure 5: Composite element of a metal-composite joint with installed load cells.

After installing the MCJ sample on the testing machine, it was pre-stretched to eliminate backlash and begin directly loading the composite part. After each loading stage, the MCJ sample was disassembled for non-destructive testing of the composite element using acoustic microscopy. The first loading stage was designed to evaluate the tensile stiffness of the loop and carbon fiber materials. Data on initial stiffness were obtained when the loop was stretched to 64 kN, which was ~26% of maximum design load P_{max} (250 kN). Fig. 6a show tensile diagrams at 65 and 100 kN, respectively, corresponding to 26 and 40% of tensile strength. The diagrams show the linear dependence of deformation δ on load P after measuring the structural gaps in the metal-composite joint, which, when stretched, amounted to 0.6–0.8 mm. The linear nature of the tension diagrams also indirectly indicates the absence of any damage to the metal-composite joint structure.

The high load-bearing capacity of the MCJ sample was experimentally confirmed by the following loading step. It was performed with loads up to 200 and 300 kN, which corresponded to 80% and 120% of the calculated breaking load P_{max}, resulting in the initial destruction of composite element structure as well as the deformation of metal bolts during connection (Fig. 6b). The deviation of the load-displacement diagram (P-δ) from linearity, when the load exceeds 260 kN, indicates the initial formation of damage, including plastic deformation in the bolts securing the metal-composite joint as well as destruction of the composite material in the loop.

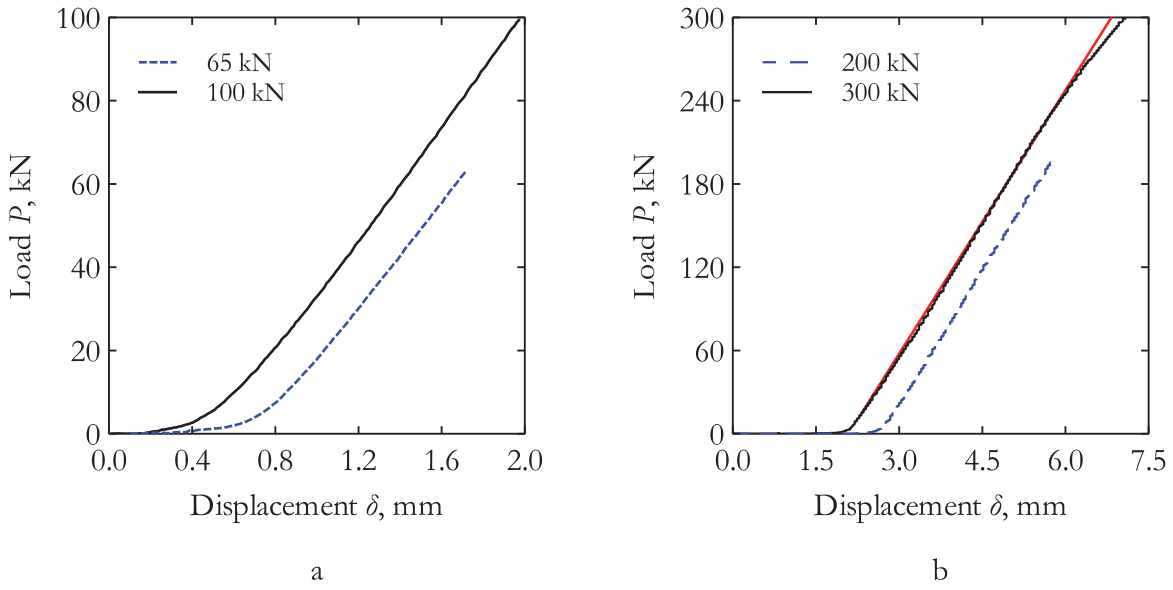

a b

Figure 6: Diagrams of the load to displacement dependence (P-δ) for the metal-composite joint prototype: a) the first stage of loading – 65 kN (26% of the design P_{max}) and 100 kN (40% of the P_{max}); b) 200 kN (80% of P_{max}) and 300 kN (120% of P_{max}).

STRESS CALCULATION USING THE FINITE ELEMENT METHOD

Finite element modeling was carried out with the standard liner method. Fig. 7 shows the calculated stress distribution from the action of the tensile force P = 250 kN, which confirms that the safety margin in the zone with the minimum thickness of the composite "loop" is 3. Such a high safety margin coefficient was established due to the non-certified properties of the composite material. The beginning of the deviations of the P-δ diagram from linearity is approximately in the calculated loading zone (Fig. 6b, red line). Experimentally, the correctness of the selected geometric parameters was confirmed, taking into account the design requirement of subsequent destruction of the composite tape only after the beginning of plastic deformation of the metal bolts in the joint. This explains the requirements for excess strength reserves of a composite element in a metal-composite joint, which guarantees the possibility of developing and implementing equal-strength metal-composite joint in the future.

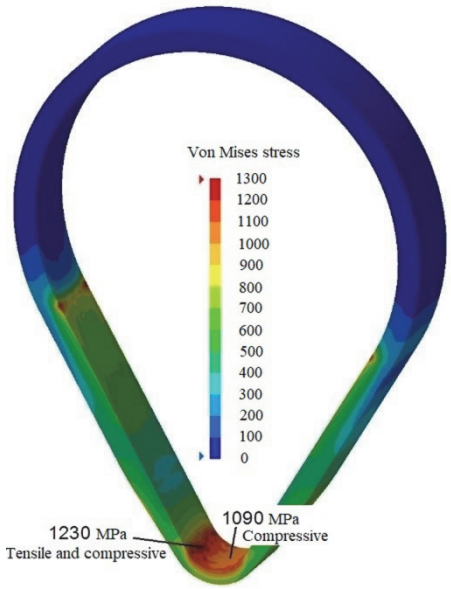

Figure 7: Calculated stress distribution in a composite element under tensile P_{max} = 250 kN.

After developing the design of the MCJ sample based on the results of the design calculation, verification calculations of the finite element method were carried out to verify the results of experimental studies, taking into account the nonlinearity of the σ-ε dependence.

Experimental studies carried out in [10] showed the effectiveness of a new generation of metal-composite joints, however, they revealed a number of loading features of such structures that require the use of a nonlinear approach to strength analysis when designing such butt joints. The loading features consisted primarily of different elastic modulus values of the composite and metal parts of the structure.

The need to use nonlinear FEM calculation models for such problems is associated with the presence of high stress gradients, which, within the framework of linear methods of strength analysis, lead to significant errors in calculations of safety factors. This paper presents the results of a study of the structural strength of new generation joints using a nonlinear engineering method intended for the initial design stage. The work used our own developed computer program [24], using an engineering technique for solving a nonlinear problem based on an iterative (step-by-step) solution of a linear problem. Research has shown that this method allows you to effectively (quickly and with high accuracy) analyze the strength of complex MCJ without a significant increase in labor intensity. The method takes into account physical and geometric nonlinearity.

Fig. 8 shows the experimentally obtained stress-strain diagram (σ-ε) based on measurements at the sticker points of load cells № 1, 2, 4 and 5 (see Fig. 5). A comparison of the experimental dependence with numerical solution, taking into account the nonlinearity, shows a satisfactory agreement. The calculations and the experiment as a whole show the nonlinearity of the σ-ε diagram with a slight increase in structural rigidity compared to the linear calculation. The weak nonlinear behavior of the structure under loading, founded in experiment, confirms the high strength properties of the MCJ structure, laid down during the design.

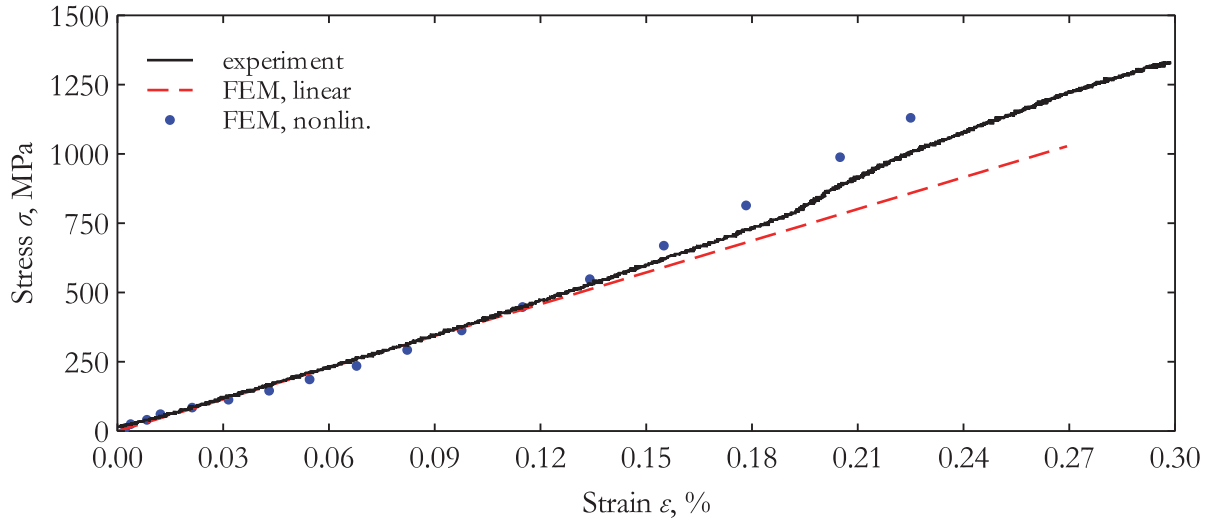

Figure 8: Stress-strain diagram (σ-ε) for the high-loaded zone of metal-composite joint. Experimental curve measured using strain cells № 1, 2, 4 and 5 in Fig. 5.

The difference between the values obtained by means of calculation and the experiment is explained by the combination of physical and geometrical nonlinear behavior of "loop" under the tension force. Initially at the small level of tension forces the difference of values related with measurement errors. As the tension force increases, fibers within the "loop" became straighter and the stiffness increases too. As the tension force increases further, geometric nonlinearity steps in this process in frame of which stresses on internal and external surfaces of "loop" are getting equals, so value of stress on external surface (where strain gauge is situated) is increasing.

ACOUSTIC VISUALIZATION OF THE COMPOSITE DAMAGES

The structure of the composite element of the MCJ was studied using a high-resolution, non-destructive technique based on a focused ultrasound impulse probe with a frequency of 50–100 MHz [20–23]. A transducer with a nominal frequency of 50 MHz and a focal distance of 13 mm in water immersion was used to study the

microstructure of PCM samples. This provided 3D imaging with a scanning step of 25 μm. Control was performed using a scanning pulse acoustic microscope with a scanning field of 250×360 mm. Damage formation in the composite structure was determined by comparing images in the initial state and after loading. Analysis was carried out layer by layer in visualization mode, in cross-sections (B-scans) and in depth planes (C-scans) as its shown in Fig. 9. The detailed principles of the applied AM method are presented in [25].

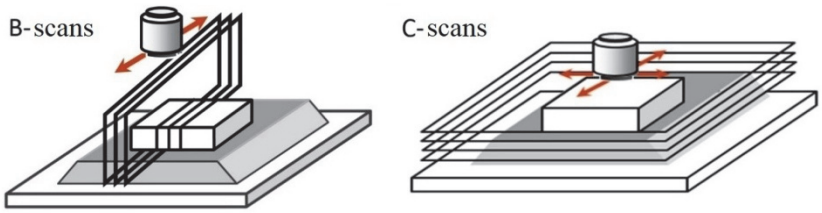

Figure 9: Scanning schemes of PCM specimens using acoustic microscope.

At the first stage before the tensile tests, the PCM samples was studied using ultrasonic microscopy. The C-scan images of the initial composite microstructure in the contact zone with the steel "tooth" were collected. Images recorded at depths of 0.25, 0.5 and 0.9 (±0.025) mm are shown in Fig. 10.

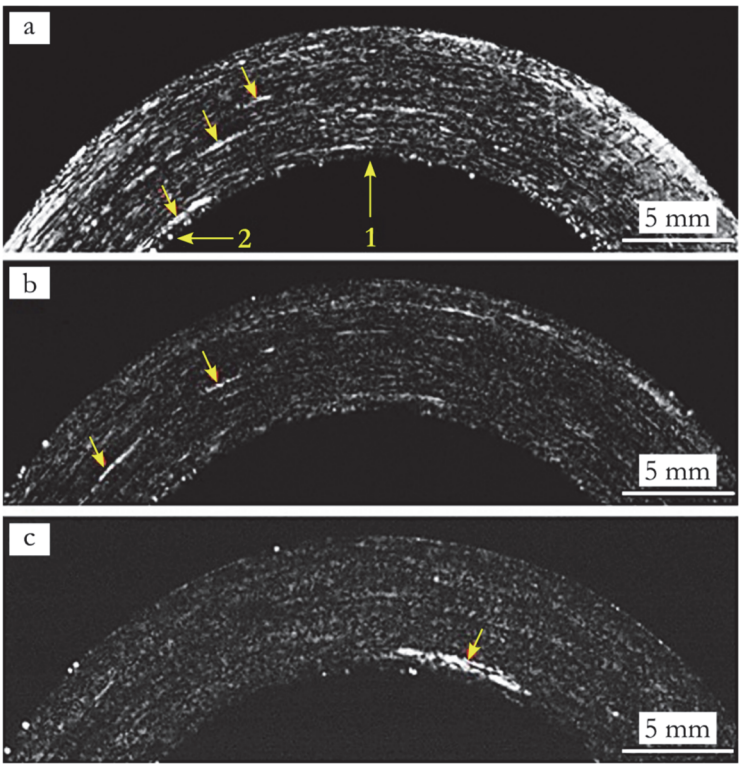

Figure 10: Acoustic images (C-scans) of the initial internal structure of the metal-composite joint element made by PCM in the contact zone with steel "tooth": a), b), and c) – depths of 0.25, 0.5, and 0.9 mm, respectively; 1 – the contact area, 2 – the transition to a regular zone. The arrows indicate technological defects.

The study of the initial structure of the connecting element in the contact zone with steel "tooth" revealed a relatively loose PCM structure, despite the preliminary compaction of this zone during the formation process to increase local strength. Numerous irregularities were visible in the images of the initial carbon fiber composite structure. They were located along the reinforcing fiber package and displayed as light contrasting with homogeneous and darker composite structures in the image. Thus, technological defects were revealed due to adhesion violations along the boundary between the carbon reinforcing filler and epoxy resin.

A sequence of acoustic images of the PCM loop in the area of the metal-composite joint after loading at 200 kN (80% of P_{max}) and 300 kN (120% of P_{max}) is presented in Fig. 11. C-scans are collected at a depth of 0.25 mm from the flat edge of

loop (Fig. 11a-c). The initial structure image is given for comparative analysis (Fig. 11a). Finally, C-scan taken at the final stage of loading (300 kN) and shifted by 50 μm towards the flat edge is given in Fig. 11d. This made it possible to observe changes or displacement of initial technological defects (Fig. 11a) during loading and deformation of the composite structure.

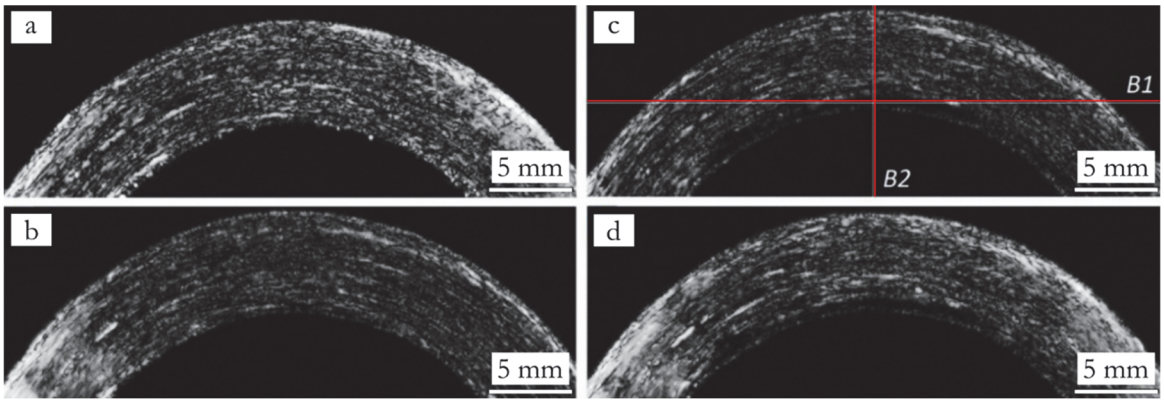

Figure 11: Acoustic images (C-scans) of composite loop structure in the loaded area: a) initial state at 0.25 mm depth; b) after 200 kN load (80% of P_{max}) at 0.25 mm depth; c) after 300 kN load (120% of P_{max}) at 0.25 mm depth; d) after a load of 300 kN (120% of P_{max}) at 0.2 mm depth.

The acoustic images in Figs. 10 and 11 shows that technological defects in the composite structure are located along fibrous packaging, and represent cavities, the largest of which are 7.5 mm long and 0.75 mm wide. When a load is applied, the fiber structure deforms, including in areas with adhesion defects. This is confirmed by Figs. 11a and 11d, which show similar identified technological defects at different depths – in the initial design they are visible at a depth of 0.25 mm (Fig. 11a), and when a load of 300 kN is applied they are seen in the plane at a distance of 0.20 mm from the edge of the composite loop, that is, they have been displaced by 50 μm towards the free edge of the metal-composite joint.

Thus, it was found that an increase in external load and the resulting compression contribute to the compaction of the composite structure. This is evidenced firstly by the change in thickness of the loop in the maximum loading zone after the start of the tests. Before the tensile test, the thickness of composite loop at the contact zone with steel "tooth" was 6.4 ± 0.025 mm, then, after loading up to 200 kN, it decreased to 6.15±0.025 mm and at 300 kN it became 5.8±0.025 mm. Additionally, the contrast of the composite structure in acoustic image decreased with constant settings and visualization depth. With reduction in structural inhomogeneity, probing ultrasonic beam becomes less scattered and reflects at irregularities.

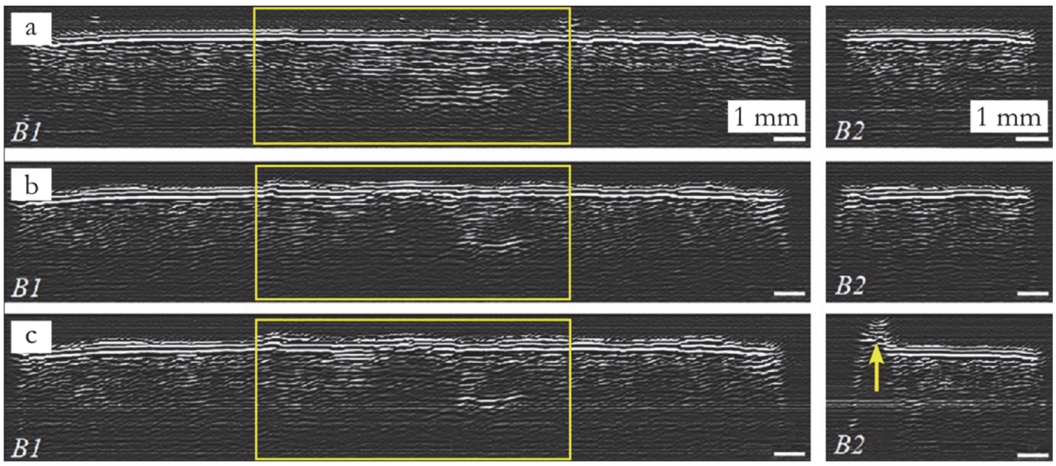

Figure 12: Acoustic images (B-scan) of fiber reinforced composite loop sample: a) initial state; b) after 200 kN load (80% of P_{max}); c) after 300 kN load (120% of P_{max}) in sections along B1 and B2 lines indicated in Fig. 11c. The arrow shows the extrusion of the polymer binder in the form of protrusion. Scale bar – 1 mm; yellow box – metal-composite joint contact zone of 10 mm length.

Fig. 12 shows acoustic cross-sections (B-scans) of a composite loop at the same location as before in the C-scans, in order to analyze in more detail, the distribution of structural damages in depth. The locations of the sections are shown in Figs. 11b – lines B1 and B2, respectively. The central part of the long B1 scan corresponds to the area with the minimum cross section of the loop, where the maximum load was applied. In short B2 scans (right side of Fig. 12), the left edge corresponds to the contact zone between the composite part and the metal tooth. In the images, one can see how defects in the original structure change as a result of applying load. Some inhomogeneities, in the form of light strokes, disappear after 200 kN load (Fig. 12b). As load increases, surface of specimen becomes increasingly rough due to extrusion of binder from composite material. Fig. 12b (on the right) shows how epoxy resin was squeezed out in the zone of maximum compression where it came into contact with the metal part of the joint. The height and width of the extruded protrusion were measured at the maximum load of 300 kN and were 0.17 and 0.5 (± 0.025) mm, respectively.

Conclusion

An engineering technique for calculating the geometric parameters of a composite element in a metal-composite joint was considered (Figs. 2–4). During design calculations, parameters for PCM element were obtained, providing the required tensile strength. This was verified using finite element method and impulse acoustic microscopy imaging. Results of static tensile tests on the MCJ prototype showed satisfactory convergence with numerical calculations, considering nonlinearity (Fig. 8). Acoustic microscopy confirmed that carbon fiber structure was not damaged at maximum design load, while deformation of composite element was accompanied by 1.1 times compaction of structure in contact zone of metal-composite joint – thickness of the loop changed from 6.4 to 5.8 mm (Fig. 11, 12). This, in turn, resulted in slight migration of technological defects and their displacement within ±0.05 mm. It was also found that the binder was squeezed out in the most stressed MCJ area, in our case by 0.17 mm towards the free edge. No other damage to the material was detected, as the applied stress (1230 MPa, Fig. 7) was near by 30% of the calculated PCM strength limits (Tab. 3). The results presented in this paper illustrate the level of damage to the PCM loop element of the metal-composite joint prototype at the early stages of mechanical loading. This approach can be useful for designing products based on lattice polymer composite structures, which include metal-composite joint, and whose reliability is highly demanded during operation.

Disclosure statement

The authors declare that they have no conflict of interest.

Acknowledgments

The work was carried out as part of a major scientific project funded by the Ministry of Science and Higher Education of the Russian Federation (Agreement No. 075-15-2024-535 dated 23 April 2024).

References

[1] Zhang, J., Lin, G., Vaidya, U. and Wang, H. (2023). Past, present and future prospective of global carbon fibre composite developments and applications, Compos. Part B: Eng., 250, 110463. DOI: https://doi.org/10.1016/j.compositesb.2022.110463

[2] Hamzat, A.K., Murad, M.S., Adediran, I.A., Asmatulu, E. and Asmatulu, R. (2025). Fiber-reinforced composites for aerospace, energy, and marine applications: an insight into failure mechanisms under chemical, thermal, oxidative, and mechanical load conditions, Adv. Compos. Hybrid Mater., 8, 152. DOI: https://doi.org/10.1007/s42114-024-01192-y

[3] Gibson, R.F. (2016). Principles of Composite Material Mechanics. CRC Press.
[4] Vasiliev, V.V. and Razin, A.F. (2006). Anizogrid composite structures for spacecraft and aircraft applications, Compos. Struct., 76(1–2), pp. 182–189. DOI: https://doi.org/10.1016/j.compstruct.2006.06.025
[5] Giusto, G., Totaro, G., Spena, P., Nicola, F. De, Caprio, F. Di, Zallo, A., Grilli, A., Mancini, V., Kiryenko, S., Das S. and Mespoulet. S. (2020). Composite grid structure technology for space applications, Mater. Today: Proc., 34(1), pp. 332–340. DOI: https://doi.org/10.1016/j.matpr.2020.05.754
[6] Hunt, C.J., Morabito, F., Grace, C., Zhao, Y. and Woods, B.K.S. (2022). A review of composite lattice structures, Compos. Struct., 284(15), 115120. DOI: https://doi.org/10.1016/j.compstruct.2021.115120
[7] Dubovikov, E., Fomin, V., Kondakov, I., Shanygin, A. and Vedernikov, D. (2018). Development of rational hybrid fuselage structure for prospective civil aircraft, Proc. Inst. Mech. Eng., Part G: J. Aerosp. Eng., 232(14), pp. 2673–2680. DOI: https://doi.org/10.1177/0954410018785501
[8] Ahmadi, H. and Rahimi, G. (2019). Analytical and experimental investigation of transverse loading on grid stiffened composite panels, Compos. Part B: Eng., 159, pp. 184–198. DOI: https://doi.org/10.1016/j.compositesb.2018.09.040
[9] Shanygin, A.N., Chernov, A.V., Fomin, D.Y., Grishin, V.I. and Kacharava I.N. (2016). Development of lightweight and reliable joints for airframes based on unidirectional composite elements, 30th Congress of the International Council of the Aeronautical Sciences (ICAS 2016), Daejeon, Korea.
[10] Chernov, A., Fomin, D., Kondakov, I., Mareskin, I. and Shanygin, A. (2018). Lightweight and reliable metal-composite joints based on harmonization of strength properties of joined parts, Proc. Inst. Mech. Eng., Part G: J. Aerosp. Eng., 232(14), pp. 2663–2672. DOI: https://doi.org/10.1177/0954410018778797
[11] Luo, B., Xue, L., Wang, Q. and Zou, P. (2024). Mechanistic study of failure in CFRP hybrid bonded-bolted interference connection structures under tensile loading, Materials, 17(9), 2117. DOI: https://doi.org/10.3390/ma17092117
[12] Ramezani, F., Simões, B.D., Carbas, R.J.C., Marques, E.A.S. and da Silva L.F.M. (2023). Developments in laminate modification of adhesively bonded composite joints, Materials, 16(2), 568. DOI: https://doi.org/10.3390/ma16020568
[13] Malekinejad, H., Carbas, R.J.C., Akhavan-Safar, A., Marques, E.A.S., Castro Sousa, F. and da Silva L.F.M. (2023). Enhancing fatigue life and strength of adhesively bonded composite joints: a comprehensive review, Materials, 16(19), 6468. DOI: https://doi.org/10.3390/ma16196468
[14] Im, J.M. and Shin, K.B. (2022). Study on the prediction method of onset and propagation of damage of unit composite lattice structure. J. Mech. Sci. Technol., 36(6), pp. 3081–3088. DOI: https://doi.org/10.1007/s12206-022-0538-3
[15] Blier, R., Monajati, L., Mehrabian, M. and Boukhili, R. (2024). Strength optimisation of hybrid bolted/bonded composite joints based on finite element analysis, Materials, 17(13), 3354. DOI: https://doi.org/10.3390/ma17133354
[16] Wang, B., Zhong, S., Lee, T., Fancey, K. and Mi, J. (2014). Non-destructive testing and evaluation of composite materials/structures: A state-of-the-art review, Adv. Mech. Eng., 12(4), 1687814020913761. DOI: https://doi.org/10.1177/1687814020913761
[17] Levin, V., Petronyuk, Y., Artyukov, I., Bukreeva, I., Malykhin, A., Longo, E., D'Amico, L., Giannoukos, K. and Tromba, G. (2023). Three-dimensional study of polymer composite destruction in the early stages, Polymers, 15(2), 276. DOI: https://doi.org/10.3390/polym15020276
[18] Ryzhova, T., Shanygin, A., Scherbakov, V., Petronyuk, Y., Levin, V. and Morokov, E. (2018). Study of external factor combinations effect on CFRP structure utilyzing ultrasonic microscopy, 31st Congress of the International Council of the Aeronautical Sciences (ICAS 2018), Belo Horizonte, Brazil.
[19] Ryzhova, T., Levin, V., Petronyuk, Y., Morokov, E. and Shanygin, A. (2019). Acoustic microscopy application for observing structural changes resulted from joint climatic and mechanical loading, International Intelligent Innovative Nondestructive testing and Evaluation Conference (INDT&E'2019), Shanghai, China.
[20] Morokov, E., Levin, V., Ryzhova, T., Dubovikov, E., Petronyuk, Y. and Gulevsky, I. (2022). Bending damage evolution from micro to macro level in CFRP laminates studied by high-frequency acoustic microscopy and acoustic emission, Compos. Struct., 288, 115427. DOI: https://doi.org/10.1016/j.compstruct.2022.115427
[21] Petronyuk, Y.S., Titov, S.A., Levin, V.M. and Ryzhova, T.B. (2021). Ultrasonic visualization of the dynamics of fracturing for reinforced composites, Bull. Russ. Acad. Sci. Phys., 85(6), pp. 642–646. DOI: https://doi.org/10.3103/S1062873821060186

[22] Pankov, A.V., Tokar, V.L., Petronyuk, Y.S., Levin, V.M., Morokov, E.S., Ryzhova, T.B. and Gulevsky, I.V. (2021). Determination of fracture toughness of carbon fiber reinforced plastics free of the crack initiator using acoustic microscopy, Inorg. Mater., 57, pp. 1519–1524. DOI: https://doi.org/10.1134/S0020168521150140

[23] Artyukov, I., Bellucci, S., Kolesov, V., Levin, V., Morokov, E., Polikarpov, M. and Petronyuk, Y. (2024). Studies of fractal microstructure in nanocarbon polymer composites, Polymers, 16(10), 1354. DOI: https://doi.org/10.3390/polym16101354

[24] Mirgorodsky, Yu.S., Mareskin, I.V., Dubovikov, E.A. and Belikov, S.E. (2023). Validation of nonlinear strength analysis based on videogrammetry method within a virtual experiment, Works TsAGI, 2819, pp. 195–199. (In Russian).

[25] Zakutailov, K.V., Levin, V.M. and Petronyuk, Y.S. (2010). High-resolution ultrasonic ultrasound methods: Microstructure visualization and diagnostics of elastic properties of modern materials (Review), Inorg. Mater., 46, pp. 1655–1661. DOI: https://doi.org/10.1134/S0020168510150100